Automotive Experiences
Vol. 8 No. 1 (2025) pp. 189-204
p-ISSN: 2615-6202 e-ISSN: 2615-6636

Research Paper

Effect of Tube Thickness Configuration of Two Segments Circular Crash Box on Its Crashworthiness Performance

Muhammad Vendy Hermawan, **Moch. Agus Choiron**, **Anindito Purnowidodo**, **Winarto**

Department of Mechanical Engineering, Universitas Brawijaya, Malang 65145, Indonesia

mvendyhermawan@student.ub.ac.id, agus_choiron@ub.ac.id

https://doi.org/10.31603/ae.13170

Published by Automotive Laboratory of Universitas Muhammadiyah Magelang

Article Info
Submitted: 12/02/2025
Revised: 24/04/2025
Accepted: 30/04/2025
Online first: 30/04/2025

Abstract

This study aims to investigate the effect of tube configuration with different bottom fixation components on the energy absorption of a two-segment crash box. The circular tube thickness configuration has two thickness levels, half of the length of the tube has thicker walls (t_2), and the other half has thinner walls (t_1). The t_1 values are 1, 1.5, 2 and 2.5 mm while t_2 is constant, 3 mm. Finite element analysis using ANSYS WORKBENCH was performed for the axial load model. The bottom fixation component uses Cutting Die Model (CDM) and Flat Model (FM). Sixteen crash box models were run to provide the effect of two tube thickness configurations and CDM-FM fixation components. The material of the circular tubes is Aluminum 6063 with a Bilinear Hardening Model assumption. Crashworthiness performance indicators were observed based on the values of Energy Absorber (EA), Specific Energy Absorber (SEA), initial peak force (F_{max}), and Crash Force Efficiency (CFE). The results show that the CDM model has the lowest F_{max} value, due to the use of the die, which stimulates easier initial folding in the tube end area. The CDM model also has better SEA and CFE values. According to the results obtained from computer simulations, the CDM-t_2t_1 model with t_1=1mm exhibited the highest Specific Energy Absorption (SEA) of 67.93 kJ. On the other hand, this same crash box model provided the smallest F_{max} of 205.88 kN and the highest CFE value of 0.69. From these results, it can be concluded that this model provides the best crashworthiness performance.

Keywords: Crash box; Circular tube; Thickness configuration; Cutting die model

1. Introduction

Trains play a pivotal role in land transportation worldwide, and their technology has undergone substantial evolution over time. As train speeds increase, the potential impact of accidents becomes more significant. Consequently, the development of effective safety features for train passengers is paramount. One promising solution involves crash boxes constructed from thin-walled tubes, serving as passive safety devices [1], [2]. These structures are widely used in the marine, transportation, and aircraft industries due to their high strength and energy absorption [3]. Factors such as cross-sectional shape [4] and constituent materials [5], [6] play a role in determining the energy absorption performance of thin-walled structures.

The high speeds of trains necessitate research into enhancing the crash energy absorption capabilities of thin-walled structures. For instance, incorporating a multi-cell plate into an energy absorber tube, with varying plate tilt angles, can significantly increase the Specific Energy Absorption (SEA) and Crash Force Efficiency (CFE) values [7]. Additionally, using multi-segment tubes with graduated thicknesses has proven effective in enhancing the energy absorption performance of thin-walled structures [8]. In related experiments, thin-walled tubes with graduated thicknesses allowed precise control over energy absorption characteristics along the tube's length [9]. Configuring tubes with up to four thickness levels results in reduced impact energy, higher SEA, improved CFE, and optimized peak force values [9]. Furthermore, adding stiffeners to thin-walled tubes has been shown to increase energy absorption by up to 90% and influence deformation patterns [10]. Bhutada conducted a study on the impact of cut-outs in circular aluminum tubes, testing both diamond and circular shapes [11]. Lee explored new design approaches for thin-walled tubes by incorporating additional structures [12]. Peng investigated the feasibility of thin-walled tube structures as energy absorbers for subway trains, applying cutting forces [13].

A novel design of a thin-walled tube crusher was developed to enhance energy absorption capability. The design can absorb 561.2 kJ of energy, surpassing the target value of 550 kJ. Surface roughness and die inclination angle have a significant effect on energy absorption [14]. The application of a die as a tube crushing method is also able to reduce the initial peak force that occurs by up to 21% [14]. Another way to increase the energy absorption of thin-walled tubes can be done by filling them with aluminum foam. Aluminum filling can increase SEA up to 6.4% [15]. In another study, single- and multi-segment circular tube crash box simulations were investigated. As a result, the crash box design with three alternating diameter segments has the best energy absorption capability [16]. Crash box research with a tubular corrugated structure has been tested and compared to the performance of the Ordinary Corrugated Tube (OCT) and Bi-tubular Corrugated Tube (BCT) types. The BCT type results in a 71% increase in energy absorption compared to the OCT type [17]. Another way to Increase the absorption ability is by adding honeycomb filling. The study compared the energy absorption characteristics of two forms of honeycomb filling, circular and hexagonal. The circular shape has a high energy absorption capacity, while the highest SEA value is achieved by the hexagonal shape [18]. Yao conducted a study of honeycomb crash boxes with eccentric loading. The results show that the structure is susceptible to instability if the horizontal offset value is more than 3 mm [19].

This study investigates the impact of tube wall thickness configuration, initial loading direction, and crushing method on the performance optimization of a thin-walled single-tube crash box. A two-thickness configuration is used in this research, where one of the thickness variables is constant, and the other thickness is the research variable. The crushing method uses the Flat Model (FM) and Cutting Die Model (CDM). The die is a crusher component expected to reduce the initial maximum force and increase energy absorption by stimulating folding at the crash box tube's end. Tests using the FM crushing method were carried out to determine the effectiveness of using CDM as a tube crushing method. Evaluation of the direction of force is carried out by applying a crash load to the end of the thinner-walled tube. The next test was carried out by applying a crash load to the end of the thick-walled tube. The implementation of the die is anticipated to initiate early folding in the end area of the crash box tube, which will help lower the F_{max} value, prevent buckling, and result in improved SEA and CFE values [20], [21]. The focus of the study is to find the most optimal performance with the combination of test parameters.

2. Method

2.1. Material and Model

The crash box tube material is made of Aluminum 6063, as referenced in previous research [9]. Material properties are obtained from tensile tests using a Universal Testing Machine (UTM) as shown in **Figure 1**. The testing was conducted using the ASTM E8M standard for tension testing of metallic materials. To perform the simulation, the properties of Al 6063 are required as input parameters. The properties of the Al 6063 material are shown in **Table 1**.

This study uses a bilinear isotropic hardening material model. The tangent modulus is required as an input parameter for the simulation. To calculate the tangent modulus, it is important to first convert the force-displacement graph from the tensile test into a stress-strain graph. The tangent modulus is obtained by calculating the slope at a point in the plastic region of the stress-strain curve. Within the linear elastic regime, the tangent modulus is equivalent to Young's modulus. However, once the material surpasses the proportional limit, the tangent modulus decreases compared to Young's modulus. This reduction occurs because the material softens and

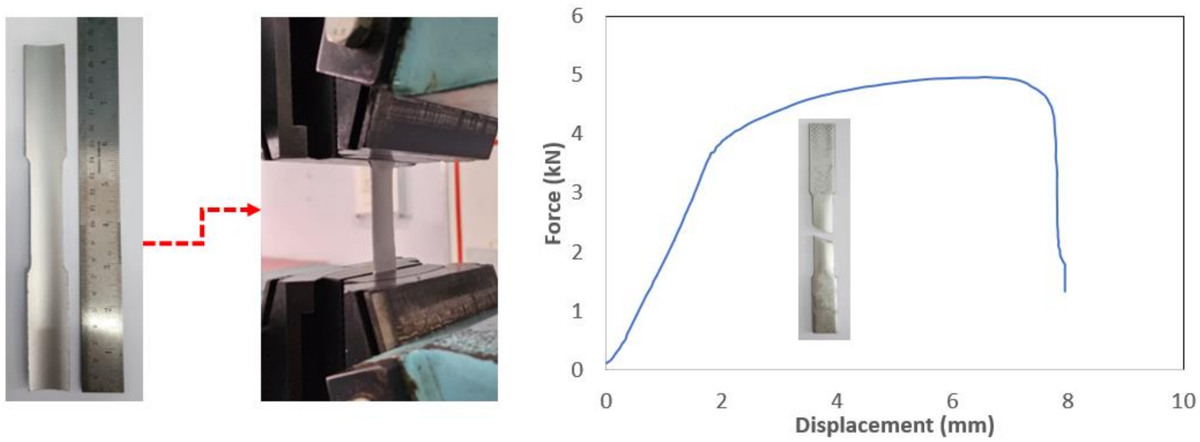

Figure 1. Force-displacement curve of Al 6063

Table 1. Properties of Al 6063

Parameters	Density (kg/m³)	Young's modulus (Gpa)	Poisson's ratio	Yield stress (MPa)	Ultimate stress (MPa)
Value	2.700	70	0.3	130.81	165.78

loses stiffness as it experiences plastic deformation. The tangent modulus can be formulated as:

$$ET = \frac{\partial\sigma}{\partial\varepsilon} \quad (1)$$

Based on test data and calculations, a tangent modulus value of 480 MPa was obtained. The research was carried out using ANSYS LD-Dyna software simulation. The 3-dimensional crash box design was created with ANSYS Design Modeler. A quadrilateral mesh is used in the simulation with a size of 5 mm. The maximum number of cycles is 1,000,000 with a time step safety factor value of 0.9. The end time of simulation is 0.1 s.

The configuration of the crash box tube thickness, crash method, and direction of the crash load are research variables. Crash box tubes have different wall thicknesses (ratio, 50%-50%), which makes the crash box tube have half the walls thin and the other half thicker. A schematic of the wall thickness of the crash box tube is shown in Figure 2. The length and diameter of the tube are 400 mm and 100 mm. The tube's length-to-diameter (L/D) ratio of 4:1 was selected based on previous studies, which indicate that this ratio is safe from buckling [10], [22]. The research uses tube wall thickness configurations of 1 – 3 mm, 1.5 – 3 mm, 2 – 3 mm, and 2.5–3 mm. The crash method is also a concern in this study. The crash method uses the Flat Model (FM) collision field and the other uses the Cutting Die Model (CDM). The frontal load was applied in two different directions: the first from the thin end of the tube (t_1), and then in the next test the direction of the load was applied to the thick part (t_2). A load of 2 tons was imposed in this research. The frontal load crash scenario was applied with reference to several previous studies [1], [8], [9], [16].

The wall thickness of the tube is shown in Figure 2, where t_2 has a constant value of 3 mm, and t_2 is the thinner wall with varying thicknesses of 1, 1.5, 2, and 2.5 mm. Analyses were done to determine the effect of different crash box tube wall thickness configurations on the crashworthiness criteria. The crash scenario uses FM and CDM crash methods. Figure 3 shows the two crash scenario methods. A new design of CDM is introduced in this study. Analyses were

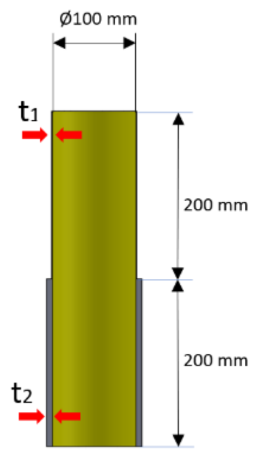

Figure 2. Crash box tube geometry

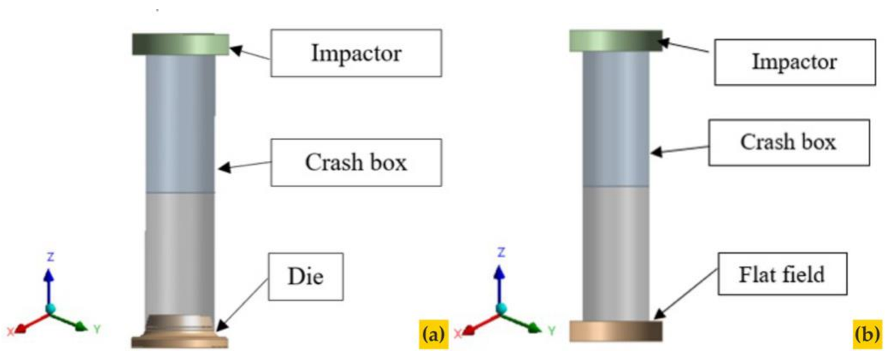

Figure 3. Tube crash methods: (a) Cutting Die Model (CDM); (b) Flat Model (FM)

done to determine the effectiveness of using CDM considering to the crashworthiness criteria for thin-walled tubes. The impactor is a rigid body representing the object that will crush the crash box, as done in previous studies [23], [24], [25], [26]. The main axis of the crash box tube and the direction of the impactor's movement are aligned with the z-axis of the coordinate system. The geometry of the die is shown in **Figure 4**. In the application, the die will be fabricated using a CNC lathe to achieve precise and accurate dimensions, closely matching the design specifications. This precision is crucial because the shape of the dies significantly influences the impact process.

In this study, the impact of load direction on a crash box composed of two segments with varying tube wall thickness was investigated. Our goal was to assess its effectiveness in enhancing crash box performance based on crashworthiness criteria. The study scenario was done using the FM and CDM crushing methods and each method uses a frontal force applied to the thin-walled tube section first (FM-t_1-t_2 and CDM-t_1-t_2). The second scenario was done by applying a frontal force to the thick-walled tube section (FM-t_2-t_1 and CDM-t_2-t_1). **Figure 5** shows the crash scenario based on the crash direction and crash box tube wall thickness configuration with two crash methods. Initial velocity represents the direction and load applied.

In this study, 16 model specimens were studied. The complete simulation specimens are shown in **Table 2**. t_2 has a constant value of 3 mm.

Boundary conditions are applied in this simulation. The impactor velocity is defined as the initial velocity. The initial velocity value is 6900 mm/s. A speed of 6900 mm/s is deemed safe for conducting crash tests, as it minimizes the risk of significant damage to the testing equipment and reduces the likelihood of serious injury to the testers [27]. Several international standards, such as EN15227 in Europe, set this speed for train crash testing to ensure consistency and facilitate

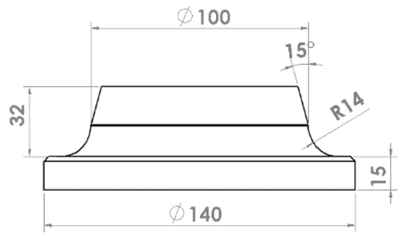

Figure 4. Die geometry (mm)

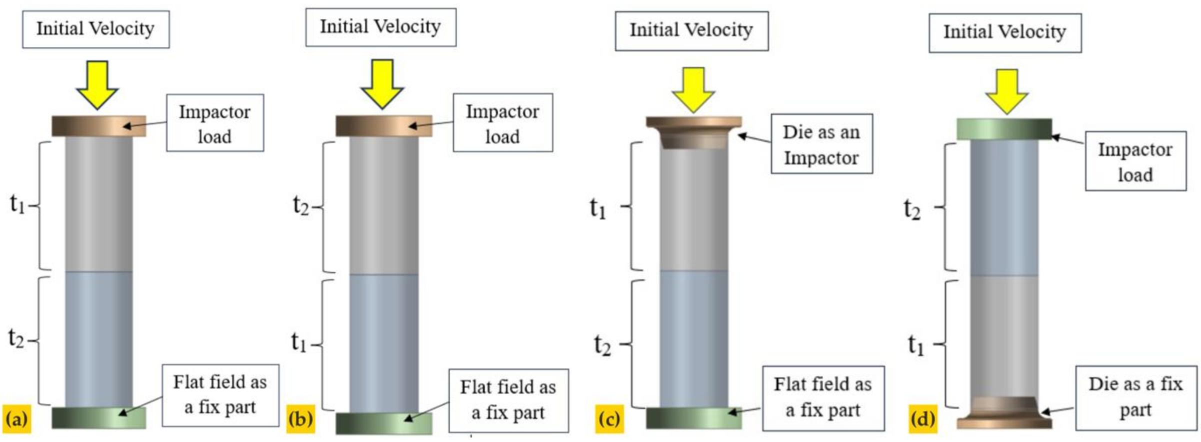

Figure 5. Crash direction scenario: (a) FM-t_1-t_2; (b) FM-t_2-t_1; (c) CDM-t_1-t2; (d) CDM-t_2t_1

Table 2. Simulation specimens

Crash method	Code		t_1 (mm)
Flat Model (FM)	FM-t_1-t_2	FM-t_2-t_1	1
	FM-t_1-t_2	FM-t_2-t_1	1.5
	FM-t_1-t_2	FM-t_2-t_1	2
	FM-t_1-t_2	FM-t_2-t_1	2.5
Cutting Die Model (CDM)	CDM- t_1-t_2	CDM- t_2-t_1	1
	CDM- t_1-t_2	CDM- t_2-t_1	1.5
	CDM- t_1-t_2	CDM- t_2-t_1	2
	CDM- t_1-t_2	CDM- t_2-t_1	2.5

easier comparison of results [28]. The load is applied in a frontal-axial direction, with a constant load value of 2 tons. The length of time applied in the simulation is 0.1s. Based on the velocity, distance, and time calculation formula, the length of time applied in the simulation is sufficient to make the impactor's final velocity equal to zero so that the energy absorption process stops. Tests were done to determine the force reaction values, deformation patterns, displacement, and internal energy. The simulation data were processed to determine the SEA, EA, F_{max}, F_{mean}, and CFE values.

2.2. *Crashworthiness Indicators*

It is important to determine the impact resistance index before starting to study the impact resistance of a crash box structure. It is necessary to evaluate crashworthiness indicators such as initial crushing force (F_{max}), average force (F_{mean}), Energy Absorption (EA), Specific Energy Absorption (SEA), Crushing Force Efficiency (CFE), and crushing deformation patterns.

2.2.1. *Energy Absorption (EA)*

EA reflects the tube's ability to absorb energy, or the total energy absorbed by a thin-walled tube in receiving an axial load. It is beneficial if the EA value is high.

$$EA = \int_0^{xn} f\,(x)dx \tag{2}$$

xn is defined as the effective crushing displacement, normally 70% to 75% of the total length of the crash box tube [29]. *F(x)* is the instantaneous axial compressive force.

2.2.2. *Specific Energy Absorption (SEA)*

SEA is the total energy absorbed per unit mass of the crash box tube. The higher SEA value, the better

$$SEA = \frac{EA}{m} \tag{3}$$

m represents the total mass of the crash box tube.

2.2.3. *F_{max}*

It shows the maximum peak force at the beginning which causes the crash box tube to start to fold. It would be good if the F_{max} value gets lower.

2.2.4. *F_{mean}*

It shows the average crushing force of the crash box tube. F_{mean} can be calculated as :

$$F_{mean} = \frac{EA}{s} \text{ or } F_{mean} \int_0^{xn} f\,(x)dx\,/xn \tag{4}$$

s is defined as the crushing distance.

2.2.5. *CFE*

It is an evaluation index of load consistency during impact. The higher the CFE, the better

$$CFE = \frac{F_{mean}}{F_{max}} \tag{5}$$

3. Results and Discussion

3.1. *Validating the Numerical Model*

To validate the numerical model in this study, it is crucial to confirm that the simulation produces accurate results. The explicit solver consistently verifies the total energy balance and tracks the distribution of energy within the system. According to the law of energy conservation, the total energy must remain constant, meaning energy can only change forms and cannot be created or destroyed. Kinetic energy results from the speed and mass of an object before a collision, represented in this study by the impactor. Internal energy is the energy absorbed by the crash box during deformation, including plastic deformation, fracture, and other mechanisms that reduce the object's kinetic energy [30].

Figure 6 shows the energy conservation graph from the CDM-t_1-t_2 (t_1=1mm) simulation. It is observed that as the internal energy curve rises, the kinetic energy begins to decrease. There is a process of energy release and absorption. The simulation is considered well-validated if the total kinetic energy equals the total internal energy. Figure 6 shows that it is evident that the kinetic and internal energy curves have the same total value. This total value is obtained by calculating the area under the curve. The total internal energy is 45.42 kJ, and the total kinetic energy has the same value. This confirms that the simulation conducted is validated.

3.2. *Effect of Crash Box Tube Wall Thickness Configuration on Crashworthiness Criteria*

An explicit dynamics simulation of the crash box crash test was conducted using ANSYS LS-Dyna software. Crash tests were used to simulate the effects on the crash box tube. Figure 7 and Figure 8 show graphs of the relationship between the force and displacement of crash box tubes with different tube thickness configurations. The initial velocity parameters and the applied load were the same in all tests. Different tube wall thickness configurations influenced differences in crushing displacement in all variables. This can be seen in Figure 7 and Figure 8. We can see that as the thickness of the tube (t_1) is reduced, the total displacement increases. Conversely, when the tube is thicker, the displacement becomes shorter. The thinner the t_1, the longer the total displacement that occurs.

Figure 7a shows the force-displacement curve for the FM-t_2-t_1 tube. The impact load is initially applied to the thin tube wall (t_1). t_1 values are 1 mm, 1.5 mm, 2 mm, and 2.5 mm, while t_2 remains constant at 3 mm. F_{max} occurs within a displacement range of 0 to 10 mm, which holds true for all thickness configuration variables. The force tends to rise again at a displacement of 200 mm, where energy is distributed to other parts of the thicker wall. However, the force does not exceed the initial peak value. FM-t_1-t_2 with t_1 = 1 mm exhibits a lower peak force and a trend in the curve, but the highest force occurs when impact energy strikes the thick wall (t_2)

Figure 7b shows the force-displacement curve for the FM-t_2-t_1 tube. The impact load on the FM is initially applied to the thick tube wall (t_2). t_1 values are 1 mm, 1.5 mm, 2 mm, and 2.5 mm, while t_2 remains constant at 3 mm. The peak force tends to be high, exceeding that of the FM-t_1-t_2 tube type. Excessive peak force is detrimental to crashworthiness criteria. The curve trend increases at a displacement of 200 mm, albeit with a moderate rise. The tube with t_1 = 1 mm exhibits the lowest force trend. An increase in the force curve corresponds to improved energy absorption, F_{mean}, and CFE. A higher CFE value is

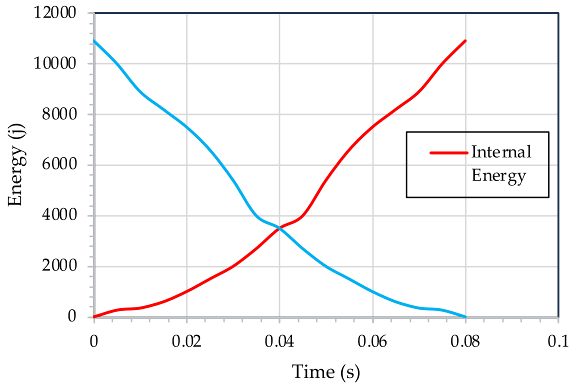

Figure 6. Curve of energy conservation numerical simulation

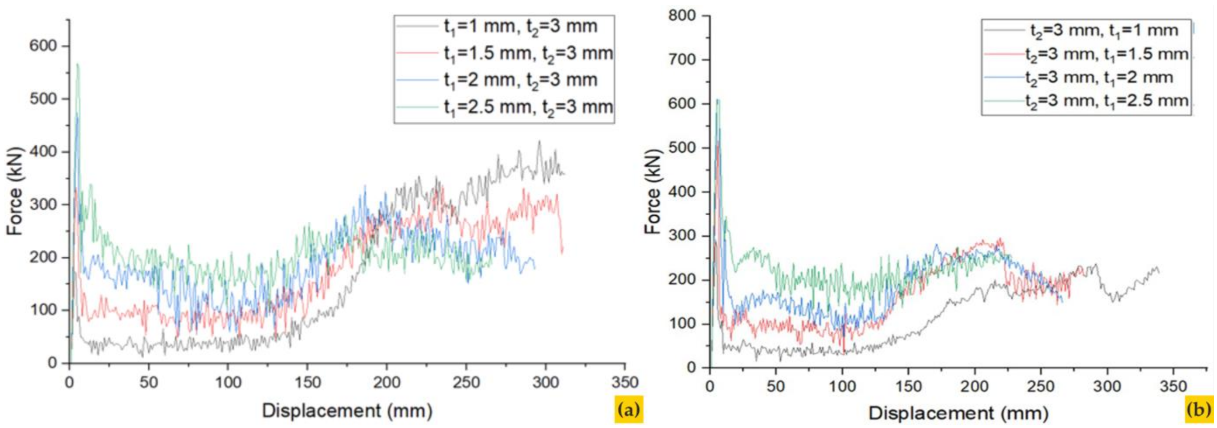

Figure 7. The curve of force-displacement FM crash methods: (a) FM-t_1-t_2; (b) FM-t_2-t_1

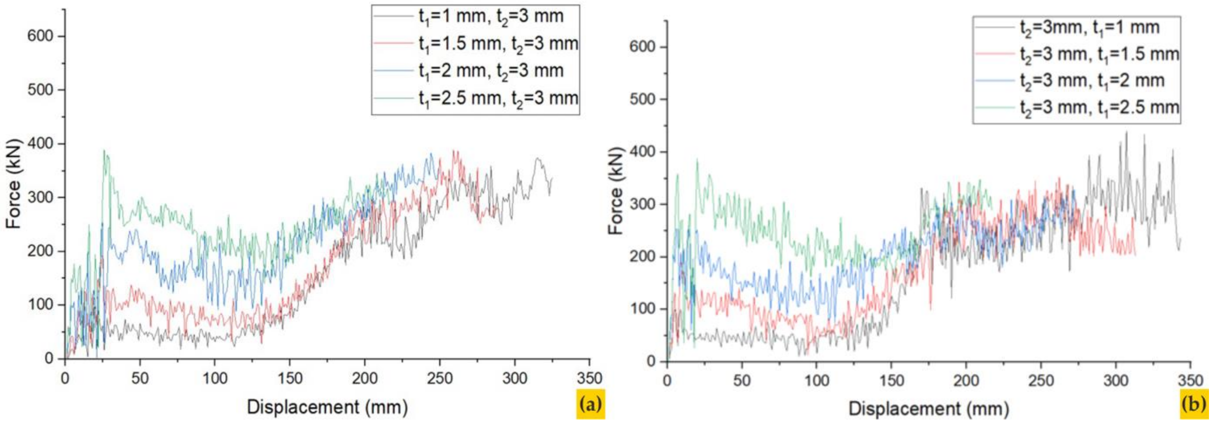

Figure 8. The curve of force-displacement CDM crash methods: (a) CDM-t_2-t_1; (b) CDM-t_1-t_2

certainly better for crashworthiness criteria [31]. However, excessively high peak forces should be avoided. Based on **Figure 7**, as the wall thickness (t_1) decreases, the initial peak force decreases, but the force increases during the second stage (when energy impacts t_2). However, the effective crush displacement distance becomes longer.

It can be concluded that the FM-t_1-t_2 configuration results in better performance. This can be seen from the lower F_{max} value and the higher force curve, which leads to an increase in EA and CFE values. Thinner t_1 will reduce F_{max} and extend displacement.

Figure 8a shows the force-displacement curve of the CDM-t_2-t_1 tube. F_{max} occurs at a displacement of 20-30 mm. Due to the initial deformation of the tube end wall by the die radius, buckling occurs. The same behavior applies to the CDM-t_1-t_2 tube (see **Figure 8b**). CDM-t_2-t_1 exhibits a lower peak force trend compared to CDM-t_1-t_2. The force increases at a displacement of 200 mm. As t_2 becomes thinner, the F_{max} value decreases. Both graphs demonstrate a significant force increase experienced by the tube with t_1 = 1 mm at a displacement of 200 mm. It is observed that specimens with thinner t_1 have a longer crash displacement.

It can be inferred that the CDM impact method yields lower peak forces compared to the FM method. The die radius enhances energy absorption by minimizing F_{max}. The initial force direction difference does not significantly affect the force-displacement curve trends for tubes t_2-t_1 and t_1-t_2. Employing a tube with two thickness segments results in a new level of increased energy absorption upon impacting the second wall thickness.

Figure 9 illustrates the reaction force response to loading as shown in the displayed force-displacement curve. The curves in **Figure 9** have been simplified by reducing the number of iterations. The response consists of two phases: the initial and secondary. The initial phase encompasses the response before failure occurs at the peak load, known as the initial peak crushing force. This response occurs at a displacement of 5-10 mm. Subsequently, changes occur through plastic failure in the crash box tube wall, forming the first folds facing outward and inward, corresponding to the response in the increase and decrease of the force-displacement curve. Folds with a constant wavelength are formed along the model. All CDM and FM models show initial crushing in the thin wall section (t_1). The next phase occurs at a displacement of 150-200 mm, where the thick wall (t_2) undergoes crushing. This increases the SEA value of the crash box. The occurrence of two sequential crushing phases is beneficial in preventing the crash box from experiencing buckling.

The parameters of reaction force and displacement are crucial components for calculating energy absorption based on Eq. (2). The values of F_{max} and displacement for energy absorption are obtained from the force-displacement curve. CFE, SEA , and F_{mean} can be determined using Eq. (3) to Eq. (5). Data on the crashworthiness indicators for the crash box multi-segment tube are shown in **Table 3.**

3.3. Influence on F_{max}, SEA and CFE

Energy absorption (EA) and specific energy absorption (SEA) are crucial parameters for evaluating crashworthiness. EA is calculated by

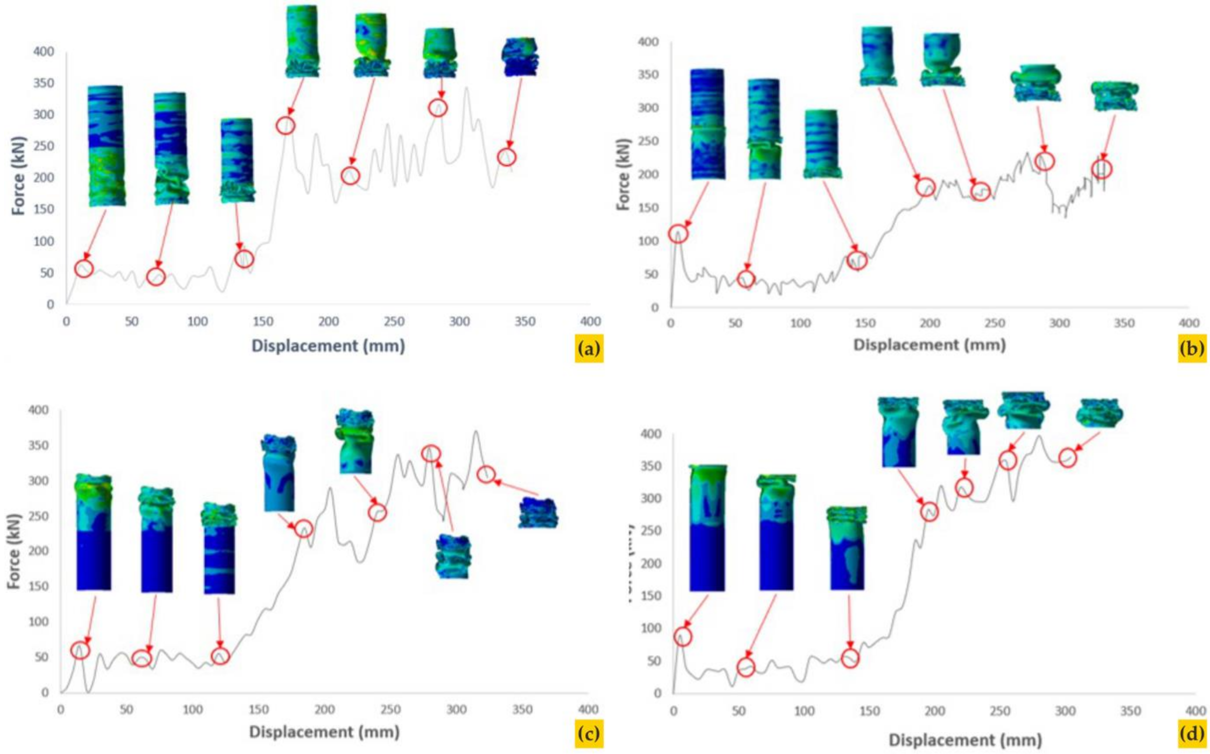

Figure 9. Force-displacement curve and deformation pattern: (a) CDM-t_2-t_1 (t1=1mm); (b) FM-t_2-t_1 (t_1=1mm); (c) CDM-t_1-t_2 (t_1=1mm); (d) FM-t_1-t_2 (t_1=1mm)

Table 3. Data of the crashworthiness indicators for the crash box multi-segment tube

Indicators	Unit	Cutting Die Model (CDM)								Mean
		t_1-t_2				t_2-t_1				
		t_1=1	t_1=1.5	t_1=2	t_1=2.5	t_1=1	t_1=1.5	t_1=2	t_1=2.5	
Mass	kg	0.70	0.78	0.87	0.96	0.70	0.78	0.87	0.96	0.83
disp.	mm	324	308	268	217	332	312	274	228	282.89
Ea	kJ	45.29	47.24	48.06	49.02	47.21	47.78	49.23	50.91	48.09
F_{max}	kN	231.00	262.20	324.00	465.00	205.88	225.00	278.00	388.7	297.47
F_{mean}	kN	139.84	153.38	179.33	225.75	142.20	153.12	179.66	223.29	174.57
CFE		0.61	0.58	0.55	0.49	0.69	0.68	0.65	0.57	0.60
SEA	kJ/kg	65.17	60.41	55.3	51.28	67.93	61.10	56.65	53.25	58.87
Indicators	**Unit**	**Flat Model (FM)**								**Mean**
		t_1-t_2				t_2-t_1				
		t_1=1	t_1=1.5	t_1=2	t_1=2.5	t_1=1	t_1=1.5	t_1=2	t_1=2.5	
Mass	kg	0.70	0.78	0.87	0.96	0.70	0.78	0.87	0.96	0.83
disp.	mm	307	297	284	264	312	277	263	225	278.72
Ea	kJ	48.06	48.89	49.56	52.34	40.32	42.77	46.84	47.47	47.04
F_{max}	kN	273.90	333.00	475.4	568.10	291.50	317.00	521.10	612.00	423.98
F_{mean}	kN	156.37	164.87	174.48	198.60	145.32	154.40	177.83	210.69	172.82
CFE		0.57	0.50	0.37	0.35	0.50	0.49	0.34	0.34	0.43
SEA	kJ/kg	69.15	62.63	57.03	54.75	58.02	54.69	53.90	49.65	57.48

determining the area under the force-displacement curve. A crash box is considered to have good crashworthiness performance when the SEA is high. Based on Equation (2), to achieve the optimal Specific Energy Absorption (SEA) value the specimen should have a minimal unit mass and a high energy absorption capacity. Table 3 shows the varying effective crushing displacements for each variable. Uniform loads and initial velocities are applied to all variables. Based on the data results in Table 3, the highest specific energy absorption (SEA) value of 67.93 kJ is associated with the CDM-t_2-t_1 tube (t_1 = 1 mm). Conversely, the FM-t_2-t_1 tube (t_1 = 2.5 mm) exhibits the lowest SEA value of 49.65 kJ. Higher SEA values correlate with improved performance. Comparing collision methods, the CDM method demonstrates a superior average SEA (58.87 kJ/kg) compared to the FM method. A comparison of SEA and CFE values of FM and CDM specimens is shown in **Figure 10**.

The FM-t₂-t₁ tube (t_1 = 2.5 mm) generates the largest F_{max} of 612 kN, while the CDM-t_2-t_1 tube (t_1 = 1 mm) has the smallest F_{max} value of 205.88 kN. Overall performance analysis reveals that the CDM crushing method yields a lower average F_{max} compared to the FM method, with average F_{max} values of 297.47 kN and 423.98 kN, respectively. This suggests that adopting the CDM method for tube crushing can effectively reduce peak force values. A comparison of F_{max} and F_{mean} values of FM and CDM specimens are shown in **Figure 11**.

CFE serves as an evaluation index for assessing crash box consistency during impact. Higher CFE values are desirable for crash boxes [9], [32]. Notably, the t_1-t_2 tube consistently exhibits superior CFE values across all crushing methods. Furthermore, when comparing crushing methods, the average CFE for the CDM method is 0.60, whereas the FM method averages 0.43. This significant difference underscores the recommendation to employ the CDM crushing method with the t_2-t_1 tube model to achieve optimal CFE.

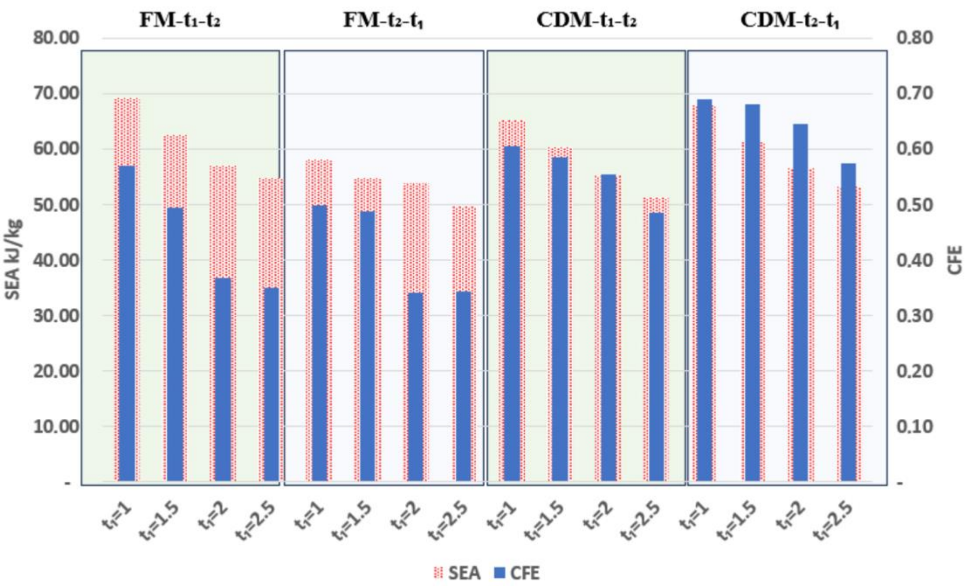

Figure 10. Comparison of SEA and CFE values of FM and CDM specimens

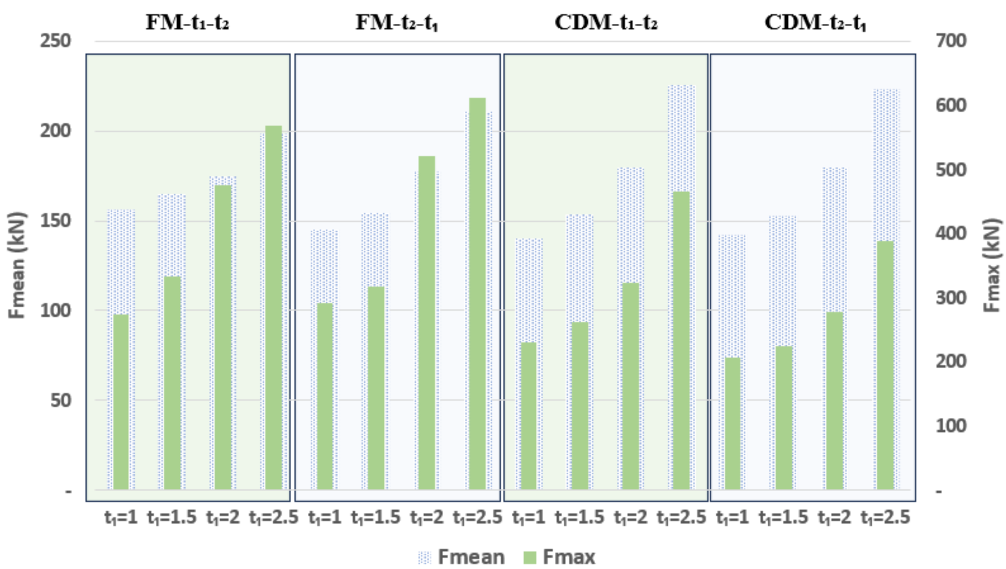

Figure 11. Comparison of F_{max} and F_{mean} values of FM and CDM specimens

Tubes with thicker walls can distribute impact forces more evenly, thereby reducing the risk of severe local damage. However, this also means a higher initial peak force because the tube is more difficult to start deforming. This phenomenon also occurs in this study, where the thicker the wall of the crash box tube, the greater the energy absorption value [33]. However, the F_{max} value also increases.

Figure 10 shows the comparison of SEA and CFE values across all specimens. It indicates that the thinner the wall thickness (t_1), the higher the SEA and CFE values. Among the model variables, the CDM model has the advantage of better CFE and SEA values. **Figure 11** shows that the CDM model tends to have a lower F_{max}. CFE is obtained from the comparison of the F_{mean} value with F_{max}. The FM model tends to have a low CFE value because the research results in a high F_{max}. Conversely, the CDM model has a higher CFE value. This results in easier and more directed folding. In previous research, an optimal F_{max} value can help increase SEA by ensuring that impact energy is effectively absorbed at the initial stage of deformation. However, if the F_{max} is too high, it can cause undesirable deformation or premature failure of the crash box, which can actually reduce the SEA value [34]. This study demonstrates that a lower F_{max} value also results in better SEA and CFE values.

The deformation behavior of a crash box under frontal loading exhibits three distinct patterns: symmetrical (concertina), asymmetrical (diamond), and a combination of both [18]. Simulation results indicate that the asymmetrical (diamond) deformation pattern is observed in all models. The diamond deformation pattern occurs because the specimen has a high length-to-diameter ratio. Tubes with a high length-to-diameter ratio tend to experience a non-axisymmetric collapse mechanism, which can result in a diamond deformation pattern [35]. This occurs due to the uneven distribution of pressure along the tube during axial loading. The diamond deformation pattern helps to enhance energy absorption capacity. The ratio between the length and diameter of the tube can influence the pressure distribution during a collision.

Crushing first occurs in the thin wall area (t_1), and this happens in all specimens. The difference in the direction of the impact force (t_1-t_2 and t_2-t_1) did not significantly affect the deformation of the tube. However, it is observed that the t_1-t_2 load direction has a higher curve when the crash process reaches the t_2 area.

Figure 12 illustrates the sequence of folding in the FM and CDM models. The FM model exhibits folding formation in the middle of the tube, specifically in the area where the thick (t_2) and thin (t_1) walls meet. Folding continues to occur in the same area along the entire length of the tube. The CDM model shows a different behavior. Initial folding occurs at the end of the tube, near the contact area with the die. The die radius stimulates the initial folding at the tube's end. Subsequently, folding continues in the same area, from the end along the entire length of the tube.

Previous research indicates that folding at the tube's end has the advantage of concentrating impact energy in a specific area, which can be beneficial in scenarios where deformation control is prioritized [22]. The initiation of folding results in a reduction of the F_{max} during a crash [36]. Folding at the tube's end effectively reduces F_{max} and prevents buckling, which could compromise the crash box's performance. In this study, it was

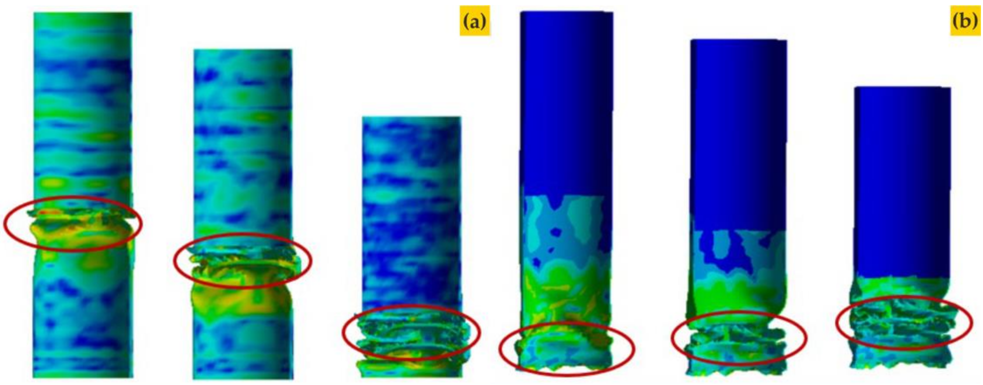

Figure 12. Sequence of the crash box tube folding: (a) FM model; (b) CDM model

found that the die plays a role in stimulating the folding at the end of the tube, which aims to reduce the F_{max} value.

The final deformation patterns of all specimens are shown in **Table 4**. Based on the observed deformation patterns, all specimens exhibit diamond deformation. Diamond deformation is characterized by a diamond-shaped pattern that forms along the crash box, typically observed under multi-axial loading conditions. This pattern not only provides good energy absorption but also helps distribute impact forces more evenly across the structure, making it beneficial in various crash scenarios [37].

While the concertina pattern is more efficient in energy absorption, the diamond deformation pattern has its advantages and is necessary for more complex crash scenarios [38]. The diamond

Table 4. The final deformation pattern of all specimens

No.	Model	t_1 (mm)	Deformation Pattern	No.	Model	t_1 (mm)	Deformation Pattern
1	FM-t_1-t_2	1	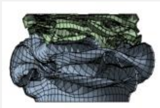	10	CDM- t_1-t_2	1.5	
2	FM-t_1-t_2	1.5	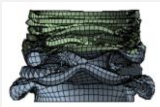	11	CDM- t_1-t_2	2	
3	FM-t_1-t_2	2	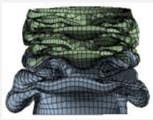	12	CDM- t_1-t_2	2.5	
4	FM-t_1-t_2	2.5		13	CDM- t_2-t_1	1	
5	FM-t_2-t_1	1		14	CDM- t_2-t_1	1.5	
6	FM-t_2-t_1	1.5		15	CDM- t_2-t_1	2	
7	FM-t_2-t_1	2		16	CDM- t_2-t_1	2.5	
8	FM-t_2-t_1	2.5		17	FM Uniform tube	(t =3 mm)	
9	CDM- t_1-t_2	1		18	CDM Uniform tube	(t =3 mm)	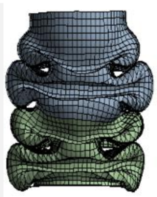

deformation pattern indicates that the crash box structure is stronger, which is crucial for its ability to absorb greater amounts of energy. This type of deformation is often found in advanced crash box designs, particularly in vehicles where a combination of strength and effective energy distribution is crucial [38].

Upon analyzing the deformation patterns across all models, variations in loading direction do not significantly affect the observed deformation behavior. Folding and fractures predominantly occur in the thin tube wall (t_1) for all testing variables. CDM results in an initial widening effect on the crash box tube diameter, particularly at the contact point with the die.

This study also compares the performance of segmented tubes with uniform tubes. A uniform tube is defined as a tube with a thickness of 3 mm (t_1=t_2=3mm). The force-displacement curve of the uniform tube can be seen in **Figure 13**. It can be observed that the graph shows an initial peak force that tends to be high, then gradually decreases until the end of the crushing process. There is no rise in the curve as seen in the segmented tube. Based on the simulation results presented in **Table 5**, the F_{max} values for the uniform tube CDM and FM models are 512.03 kN and 721.11 kN. Respectively, making both have higher F_{max} values compared to all other models. High F_{max} values are not favorable for crashworthiness performance. High F_{max} values result in low CFE, and greater thickness increases the mass of the tube, leading to low SEA. **Table 5** presents the performance results of the uniform tube, showing that the SEA and CFE values are lower than those of the multi-segment tube. The SEA values for the FM and CDM models are 51.22 kJ/kg and 47.91 kJ/kg. CFE values are 0.38 and 0.48. These results indicate that the crashworthiness performance of the multi-segment tube is still better than that of the uniform tube.

4. Conclusion

This study investigated the effects of tube wall thickness, segment configuration, crash method, and load direction on crashworthiness criteria. Based on simulations and data analysis, it can be concluded that the CDM impact method exhibits a lower F_{max} compared to the FM method. The die radius shape enhances energy absorption by minimizing the F_{max}. The initial force direction difference does not significantly affect the force-displacement trend between tube segments t_2-t_1

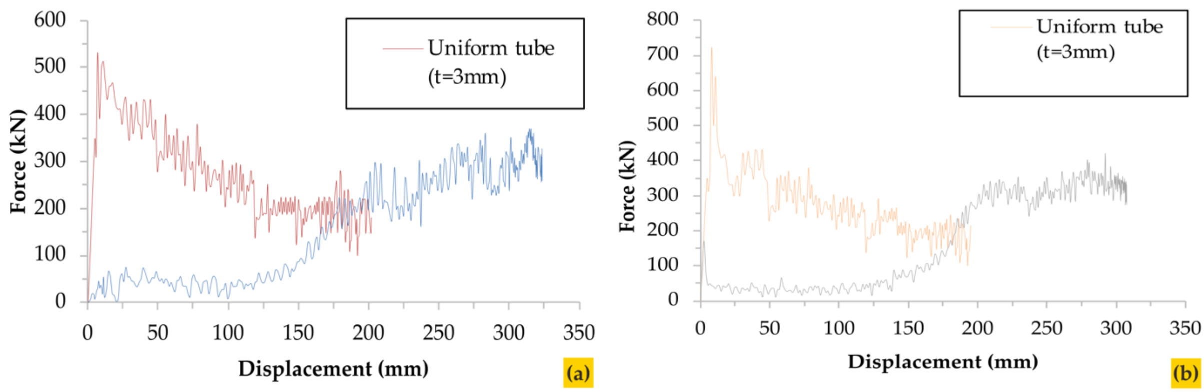

Figure 13. Comparison of the force-displacement curves of uniform and multi-segment tubes : (a) CDM model; (b) FM model

Table 5. Data of the crashworthiness indicators for the crash box uniform tube

Indicators	Unit	Uniform tube (t=3mm)	
		FM	CDM
Mass	kg	1.05	1.05
disp.	mm	195	203
Ea	kJ	53.78	50.31
F_{max}	kN	721.11	512.03
F_{mean}	kN	276.29	247.88
CFE		0.38	0.48
SEA	kJ/kg	51.22	47.91

and t_1-t_2. Furthermore, using a two-segment tube thickness results in an increased EA upon impacting the second wall thickness. The results indicate that variations in the wall thickness of the crash box tube significantly enhance the energy absorption (EA) value. The thin wall (t_2) effectively prevents buckling during crushing, while the thick wall (t_1) increases the EA value. The crash deformation method (CDM) influences the initial deformation, with folding occurring at the tube's end in the contact area with the die, leading to a reduction in the F_{max}. The loading direction does not significantly impact the deformation behavior. This study demonstrates that the deformation phenomenon consistently begins in the thin wall (t_2) across all loading directions. The CDM impact method yields a higher average SEA value (67.93 kJ/kg) compared to the FM method. Additionally, the CDM demonstrates a lower average F_{max} value than FM. Specifically, the average F_{max} for the CDM crusher method is 297.47 kN, while for FM, it is 423.98 kN. This suggests that utilizing a die as a tube-crushing method effectively reduces the maximum peak force. Furthermore, the CFE averages 0.60 for CDM and 0.43 for FM. The significant difference indicates that the CDM crusher method is recommended for achieving favorable SFE values. Notably, the highest CFE value of 0.69 is associated with the CDM-t_2-t_1.tube configuration. The results of this study indicate that the initial folding at the end of the tube is stimulated by the presence of a die. This phenomenon reduces the F_{max} value and increases the SEA because the energy absorption during the crash becomes more efficient. Increase the thickness of the tube can be done to increase SEA. However, this also results in a higher F_{max}. Therefore, the selection of wall thickness parameters needs to be adjusted according to the requirements.

Acknowledgments

The author expresses gratitude to PT INKA Madiun, Indonesia, for their support and cooperation in this research. Also, thanks are extended to Universitas Brawijaya Malang, Indonesia, and Sekolah Tinggi Teknologi Warga Surakarta, Indonesia, for providing facilities, assistance, and invaluable support.

Author's Declaration

Authors' contributions and responsibilities

M. V. H, M. A. C: the authors significantly contributed to the study's conception and design; M. V. H, M. A. C, A. P: the authors were responsible for and actively participated in data analysis, interpretation, and discussion of the results; M. A. C, A. P, W. : the authors reviewed and approved the final manuscript.

Funding

No funding information from the authors.

Availability of data and materials

All data are available from the authors.

Competing interests

The authors declare no competing interest.

Additional information

No additional information from the authors.

References

[1] W. Guan, Y. Yu, and G. Gao, "Crashworthiness performance and multiobjective optimization of a combined splitting circular tube energy absorber under eccentric impact for subway vehicles," *International Journal of Impact Engineering*, vol. 158, no. October 2020, p. 104006, 2021, doi: 10.1016/j.ijimpeng.2021.104006.

[2] J. Xing *et al.*, "Crashworthiness optimisation of a step-like bi-tubular energy absorber for subway vehicles," *International Journal of Crashworthiness*, vol. 25, no. 3, pp. 252–262, 2020, doi: 10.1080/13588265.2019.1577522.

[3] J. Xing, P. Xu, S. Yao, H. Zhao, Z. Zhao, and Z. Wang, "Study on the layout strategy of diaphragms to enhance the energy absorption of thin-walled square tubes," *Structures*, vol. 29, no. December 2020, pp. 294–304, 2021, doi: 10.1016/j.istruc.2020.11.024.

[4] N. S. Ha, T. M. Pham, W. Chen, H. Hao, and G. Lu, "Crashworthiness analysis of bio-inspired fractal tree-like multi-cell circular tubes under axial crushing," *Thin-Walled Structures*, vol. 169, no. August, p. 108315, 2021, doi: 10.1016/j.tws.2021.108315.

[5] T. S. Sachit and N. Mohan, "Wear rate optimization of tungsten carbide (WC) nano particles reinforced aluminum LM4

alloy composites using Taguchi techniques," *Materials Research Express*, vol. 6, no. 6, p. 066564, Mar. 2019, doi: 10.1088/2053-1591/ab0e3f.

[6] G. Sun, X. Guo, S. Li, D. Ruan, and Q. Li, "Comparative study on aluminum/GFRP/CFRP tubes for oblique lateral crushing," *Thin-Walled Structures*, vol. 152, no. August 2019, p. 106420, 2020, doi: 10.1016/j.tws.2019.106420.

[7] M. S. Zahran, P. Xue, and M. S. Esa, "Novel approach for design of 3D-multi-cell thin-walled circular tube to improve the energy absorption characteristics under axial impact loading," *International Journal of Crashworthiness*, vol. 22, no. 3, pp. 294–306, 2017, doi: 10.1080/13588265.2016.1258958.

[8] C. Baykasoglu and M. T. Cetin, "Energy absorption of circular aluminium tubes with functionally graded thickness under axial impact loading," *International Journal of Crashworthiness*, vol. 20, no. 1, pp. 95–106, 2015, doi: 10.1080/13588265.2014.982269.

[9] S. Xie, S. Zheng, J. Zhang, Z. Liu, and H. Zhou, "The design of circular tubes with stepped varying thicknesses and their synergistic multi-tube combination," *Structures*, vol. 57, no. June, p. 105125, 2023, doi: 10.1016/j.istruc.2023.105125.

[10] M. D. Goel, "Numerical investigation of the axial impact loading behaviour of single, double and stiffened circular tubes," *International Journal of Crashworthiness*, vol. 21, no. 1, pp. 41–50, 2016, doi: 10.1080/13588265.2015.1113617.

[11] S. Bhutada and M. D. Goel, "Study of effect of provision of cut-outs on axial collapse behaviour of circular aluminium tubes," *International Journal of Impact Engineering*, vol. 178, no. January, p. 104599, 2023, doi: 10.1016/j.ijimpeng.2023.104599.

[12] W. Lee *et al.*, "Effect of auxetic structures on crash behavior of cylindrical tube," *Composite Structures*, vol. 208, no. October 2018, pp. 836–846, 2019, doi: 10.1016/j.compstruct.2018.10.068.

[13] Y. Peng, S. Wang, S. Yao, and P. Xu, "Crashworthiness analysis and optimization of a cutting-style energy absorbing structure for subway vehicles," *Thin-Walled Structures*, vol. 120, no. August, pp. 225–235, 2017, doi: 10.1016/j.tws.2017.09.006.

[14] D. M. Costescu, A. Hadăr, and S. D. Pastramă, "A new solution for impact energy dissipation during collision of railway vehicles," *Materials Today: Proceedings*, vol. 32, pp. 72–77, 2019, doi: 10.1016/j.matpr.2020.02.336.

[15] S. Wang, M. Zhang, W. Pei, F. Yu, and Y. Jiang, "Energy-absorbing mechanism and crashworthiness performance of thin-walled tubes diagonally filled with rib-reinforced foam blocks under axial crushing," *Composite Structures*, vol. 299, no. January, p. 116149, 2022, doi: 10.1016/j.compstruct.2022.116149.

[16] M. A. Choiron, A. Purnowidodo, E. S. Siswanto, and N. A. Hidayati, "Crash energy absorption of multi-segments crash box under frontal load," *Jurnal Teknologi*, vol. 78, no. 5, pp. 347–350, 2016, doi: 10.11113/jt.v78.8334.

[17] I. Choirotin, M. A. Choiron, A. Purnowidodo, and D. B. Darmadi, "Deformation Mode and Energy Absorption Analysis of Bi-Tubular Corrugated Crash Box Structure," *International Journal of Integrated Engineering*, vol. 13, no. 5, pp. 274–280, 2021, doi: 10.30880/ijie.2021.13.07.031.

[18] M. A. Choiron, "Characteristics of deformation pattern and energy absorption in honeycomb filler crash box due to frontal load and oblique load test," *Eastern-European Journal of Enterprise Technologies*, vol. 2, no. 7–104, pp. 6–11, 2020, doi: 10.15587/1729-4061.2020.200020.

[19] S. Yao, X. Xiao, P. Xu, Q. Qu, and Q. Che, "The impact performance of honeycomb-filled structures under eccentric loading for subway vehicles," *Thin-Walled Structures*, vol. 123, no. October 2017, pp. 360–370, 2018, doi: 10.1016/j.tws.2017.10.031.

[20] A. Borse, R. Gulakala, and M. Stoffel, "Multi-parameter design optimization of crash box for crashworthiness analysis," *PAMM*, vol. 24, no. 3, Oct. 2024, doi: 10.1002/pamm.202400096.

[21] F. Xiong, Z. Wang, D. Wang, L. Ji, H. Wu,

and X. Zou, "Multi-objective robust optimization of foam-filled double-hexagonal crash box using Taguchi-grey relational analysis," *Advances in Mechanical Engineering*, vol. 15, no. 8, pp. 1–24, 2023, doi: 10.1177/16878132231189070.

[22] A. Jusuf *et al.*, "Design Exploration and Optimization of a Multi-Corner Crash Box under Axial Loading via Gaussian Process Regression," *International Journal of Technology*, vol. 15, no. 6, p. 1749, Dec. 2024, doi: 10.14716/ijtech.v15i6.7278.

[23] S. Widi Astuti, W. Artha Wirawan, A. Zulkarnain, and D. Tri Istiantara, "Comparison of Energy Absorption and Pattern of Deformation Material Crash Box of Three Segments with Bilinear and Johnson Cook Approach," *Journal of Physics: Conference Series*, vol. 1273, no. 1, 2019, doi: 10.1088/1742-6596/1273/1/012078.

[24] W. A. Wirawan *et al.*, "Collapse Behavior and Energy Absorption Characteristics of Design Multi-Cell Thin Wall Structure 3D-Printed Under Quasi Statistic Loads," *Automotive Experiences*, vol. 7, no. 1, pp. 149–160, May 2024, doi: 10.31603/ae.10892.

[25] C. J. G. Silva, R. F. F. Lopes, T. M. R. M. Domingues, M. P. L. Parente, and P. M. G. P. Moreira, "Crashworthiness topology optimisation of a crash box to improve passive safety during a frontal impact," *Structural and Multidisciplinary Optimization*, vol. 68, no. 1, 2025, doi: 10.1007/s00158-024-03924-6.

[26] Harikrishna and N. A. Sakle, "Design and Analysis of Compatibility of Crash Box with Trigger and Thickness Variation for Vehicle Frontal Part During Low Velocity Collision," *International Journal of Scientific Research and Engineering Trends*, vol. 7, no. 4, pp. 2890–2895, 2021.

[27] Z. Z. Li, T. Zhu, S. N. Xiao, J. K. Zhang, X. R. Wang, and H. X. Ding, "Simulation method for train curve derailment collision and the effect of curve radius on collision response," *Proceedings of the Institution of Mechanical Engineers, Part F: Journal of Rail and Rapid Transit*, vol. 237, no. 9, pp. 1130–1139, 2023, doi: 10.1177/09544097231154313.

[28] F. I. Tovey, "Publishing Agreement," *Diabetic Medicine*, vol. 1, no. 1, pp. 72–72, 1984, doi: 10.1111/j.1464-5491.1984.tb01928.x.

[29] W. Abramowicz and N. Jones, "Dynamic progressive buckling of circular and square tubes," *International Journal of Impact Engineering*, vol. 4, no. 4, pp. 243–270, Jan. 1986, doi: 10.1016/0734-743X(86)90017-5.

[30] R. Fajri, H. L. Guntur, and R. Apriadi, "Analysis High Energy Absorption and Numerical Study of Crashbox," *International Journal of Engineering Research and Technology (IJERT)*, vol. 13, no. 5, 2024, doi: 10.17577/IJERTV13IS050303.

[31] L. Wei, L. Zhang, X. Tong, and K. Cui, "Crashworthiness study of a subway vehicle collision accident based on finite-element methods," *International Journal of Crashworthiness*, vol. 26, no. 2, pp. 159–170, 2021, doi: 10.1080/13588265.2019.1699742.

[32] X. Luo, J. Xu, J. Zhu, Y. Gao, L. Nie, and W. Li, "A new method to investigate the energy absorption characteristics of thin-walled metal circular tube using finite element analysis," *Thin-Walled Structures*, vol. 95, pp. 24–30, 2015, doi: 10.1016/j.tws.2015.06.001.

[33] R. Ardiansyah, F. K. Indriani, D. Hidayat, A. Tjahjono, A. Nurrohmad, and A. Marta, "Crashworthiness Performance Study of 3D-Printed Multi-Cell Tubes Hybridized with Aluminum Under Axial Quasi-Static Testing," *Automotive Experiences*, vol. 7, no. 3, pp. 567–578, Dec. 2024, doi: 10.31603/ae.12247.

[34] W. A. Wirawan *et al.*, "Crashworthiness characteristic of aluminum/composite hybrid tubes under axial compression," *Results in Engineering*, vol. 25, no. January, 2025, doi: 10.1016/j.rineng.2024.103889.

[35] M. A. Choiron, "Energy Absorption and Deformation Pattern Analysis of Initial Folded Crash Box Subjected to Frontal Test," *Journal of Energy, Mechanical, Material and Manufacturing Engineering*, vol. 2, no. 1, p. 1, 2017, doi: 10.22219/jemmme.v2i1.4689.

[36] J. Marzbanrad, A. Abdollahpoor, and B. Mashadi, "Effects of the triggering of circular aluminum tubes on crashworthiness," *International Journal of*

Crashworthiness, vol. 14, no. 6, pp. 591–599, 2009, doi: 10.1080/13588260902896458.

[37] H. Rostro-González, J. M. Puigoriol-Forcada, A. Pérez-Peña, J. Menacho, and A. A. Garcia-Granada, "Optimizing crash box design to meet injury criteria: a protocol for accurate simulation and material selection," *Structural and Multidisciplinary Optimization*, vol. 67, no. 8, pp. 1–17, 2024, doi: 10.1007/s00158-024-03855-2.

[38] X. Y. Ang *et al.*, "Evaluation of Automotive Bio-Composites Crash Box Performance," *International Journal of Automotive and Mechanical Engineering*, vol. 20, no. 4, pp. 10943–10952, 2023, doi: 10.15282/ijame.20.4.2023.11.0846.